Characterizing Asphaltene Deposition in the Presence of Chemical Dispersants in Porous Media Micromodels

Yu-Jiun Lin[1], Peng He[1], Mohammad Tavakkoli[1], Nevin Thunduvila Mathew[2], Yap Yit Fatt[3], John C. Chai[4], Afshin Goharzadeh[3], Francisco M. Vargas[1], and Sibani Lisa Biswal[1*]

[1]Department of Chemical and Biomolecular Engineering, Rice University, Houston, Texas 77005, United States

[2]Department of Chemical Engineering, The Petroleum Institute, Post Office Box 2533, Abu Dhabi, United Arab Emirates

[3]Department of Mechanical Engineering, The Petroleum Institute, Post Office Box 2533, Abu Dhabi, United Arab Emirates

[4]School of Computing and Engineering, University of Huddersfield, Huddersfield HD1 3DH, United Kingdom

*Email: biswal@rice.edu

Abstract

Asphaltenes are components in crude oil known to deposit and interrupt flows in critical regions during oil production, such as the wellbore and transportation pipelines. Chemical dispersants are commonly used to disperse asphaltenes into smaller agglomerates or increase asphaltene stability in solution with the goal of preventing deposition. However, in many cases, these chemical dispersants fail in the field or even worsen the deposition problems in the wellbores. Further understanding of the mechanisms by which dispersants alter asphaltene deposition under dynamic flowing conditions are needed to better understand flow assurance problems. Here, we describe the use of porous media microfluidic devices to evaluate how chemical dispersants change asphaltene deposition. Four commercially used alkyl-phenol model chemical dispersants are tested with model oils flowing through porous media, and the resulting deposition kinetics are visualized at both the matrix-scale and the pore-scale. Interestingly, initial asphaltene deposition worsens in the presence of the tested dispersants, but the mechanism by which plugging and permeability reduction in the porous media varies. The velocity profiles near the deposit are analyzed to further investigate how shear forces affect asphaltene deposition. The deposition tendency is also related to the intermolecular interactions governing the asphaltene-dispersant systems. Furthermore, the model system is extended to a real case. The use of porous media microfluidic devices offers a unique

platform to develop and design effective chemical dispersants for flow assurance problems.

1. Introduction

Flow assurance in the oil and gas industry has been focused on preventing asphaltene deposition.[1–6] Severe asphaltene problems often arise in the porous media near the wellbore region, where significant changes either in shear rates or pressure occur. As a result of these flow changes, nano- and micro-aggregates of the destabilized asphaltenes form in the crude oil.[7,8] Additionally, temperature and composition of the crude oil can also vary significantly during crude oil recovery, causing asphaltenes to precipitate. In particular, pipeline fouling has been reported to be a result of CO_2 injection in Enhanced Oil Recovery (EOR)[9,10] and mixing various crude oil streams.[11] Following initial adsorption, asphaltene deposition can cause flow assurance problems by plugging small pore throats via the mechanical trapping or depositing on rock surfaces.[12,13] Both plugging and non-plugging depositions contribute to the permeability reduction within the porous media. Depending on the local flow velocity gradients, asphaltene deposits can be mobilized from non-plugging deposits to later contribute to mechanical trapping and plugging of the porous media, which further depicts the complexity of asphaltene deposition to flow assurance.

Common solutions utilized to tackle this problem include mechanical removal using scrapers or solvent washing in the wellbore and near-wellbore region.[14,15] Additionally, preventive chemical additives, such as asphaltene inhibitors or dispersants, have been

proposed to be injected into the wellbore and formation. Inhibitors can be used to shift the thermodynamic conditions required for asphaltene precipitation versus dispersants prevent destabilized asphaltene agglomerates from flocculating and aggregating with the goal of keeping asphaltenes suspended in the crude oil so that they can be carried by the flow instead of depositing onto the surface or plugging pore throats.[16–21] Previous studies of low-molecular-weight alkylbenzene-derived amphiphile dispersants investigate the influence of both the polarity of head groups and length of the alkyl tail on stabilizing asphaltenes under the scenario that polar moiety attaches to asphaltenes, and alkyl tails offer steric repulsion.[16,17] Bulk studies of alkylphenol dispersants on the asphaltene aggregation in heptane/toluene (Heptol) solutions evaluated dispersant effectiveness in terms of delaying the precipitation onset and reducing aggregate size.[22] The effectiveness of dispersants is typically characterized by quantifying the concentration of suspended asphaltenes in the solution using turbidity measurements and dispersancy tests by transmittance under static conditions.[16,17,22–27] However, the performance of dispersants under complex flow conditions is difficult to predict solely from static dispersancy tests. Without considering hydrodynamic effects on asphaltene aggregates, these chemical dispersants may worsen deposition and hasten flow assurance problems in the field.[28] Although commercially available alkyl-phenols have demonstrated various successes as asphaltene dispersants, it is not clear how these chemicals influence plugging and non-plugging asphaltene deposition processes. Therefore, it is

important to study the performance of asphaltene dispersants under flowing conditions in porous media and integrate these studies with conventional dispersancy tests to form a multifaceted screening platform to better understand the influence of chemical additive injections for flow assurance.

Microfluidic systems provide a fast and well-controlled platform to study flow processes within porous media, and to date, has been successfully applied to various crude oil and asphaltene systems.[29–33] The typical length scales of microfluidic devices match the representative pore sizes of the near-wellbore region and reservoir rock, and its transparency allows processes to be visualized.[34–36] The direct visualization capacity provide a platform for studying asphaltene deposition dynamics in great detail. Additionally, the high surface-to-volume ratio in microfluidic devices gives rise to a highly controllable measurement for studying particle-surface interactions and provides a high-throughput platform for efficient screening of dispersants. Deposition is a result of competition between surface adsorption and erosion. Adsorption is dominated by the diffusion of small asphaltene particles to the surface, but erosion is governed by the shear forces exerted by fluid convection acting on the deposited aggregates. The convection-diffusion effect has been previously highlighted as an important factor on asphaltene deposition.[37] In this study, dispersants alter the size and the intermolecular interactions between asphaltene aggregates; hence influencing both the diffusion and shear removal regarding the deposition process.

In this paper, we studied the deposition kinetics of asphaltenes under the influence of dispersants with dynamic flow conditions in porous media microfluidic devices. In particular, we will identify how various chemical dispersants changes the effective asphaltene size and intermolecular interactions, which in turn alters the deposition and shear removal tendencies. A microfluidic device was used to analyze different asphaltene deposition growth rates and morphologies and provides further insight how altering the chemical interactions among asphaltenes can lead to worsening deposition in porous media.

2. Experimental Methods

2.1 Asphaltenes in Model Oils and Crude Oil with Dispersants

The asphaltenes used in this study were extracted from Canadian bitumen samples by *n*-pentane. A model oil was prepared by slowly dissolving the extracted asphaltenes in toluene at 90^{o}C in 40 kHz ultrasonication bath (Branson) for a minimum of 30 minutes until a final asphaltene concentration of 0.5 wt% was reached. Results with the model oil are also compared with Crude Oil S, whose properties at 1 atm and 23 ^{o}C are listed in Table 1. Commercial dispersants, such as *p*-dodecylphenol (purity ≥ 96.5%) [Pfaltz & Bauer (Connecticut, USA)], *p*-hexylphenol (98%), *p*-octylphenol (99%), *iso*-dodecylphenol and other chemicals were reagent grade (purity ≥ 99%) [Sigma-Aldrich (Missouri, USA)] and used as is. These various dispersants were premixed into the model oil at the concentration of 0.01 wt%, characteristic of what would typically be used in field applications. A gravimetric

and spectroscopic measurement[38] on the model oils confirmed that the dispersants did not precipitate additional asphaltenes from the model oil.

Table 1. Properties of Crude Oil S

Density (g/cm^3)	0.826
Viscosity (cP)	5.36
Saturates (wt %)	69.60
Aromatics (wt %)	22.02
Resins (wt %)	7.17
C5 asphaltenes (wt %)	1.21

The required amount of anti-solvent to induce asphaltene precipitation is a measure of the stability of the asphaltenes in the oil phase. Titration with *n*-heptane combined with gravimetric and spectroscopic measurements was used to determine that the instantaneous precipitation point of asphaltenes from the model oil occurred at 45 vol% of *n*-heptane. It is important to note that previous research has shown that this phase separation is a dynamic process, which indicates that the instantaneous precipitation point is time-dependant.[39,40] Therefore, the instantaneous precipitation point measured occurred at approximately 10 minutes, which is the timescale for which oil would contact the porous media. Asphaltenes were forced to precipitate out of the model oil by mixing with *n*-heptane at the volumetric ratio of 20:80, which was well above the instantaneous precipitation point. Zeta potential and dynamic light scattering (DLS) measurements were performed using a Delsamax Pro (Beckman Coulter) instrument to estimate the effective size and the charge of asphaltene

aggregates in the absence and presence of the various dispersants. Samples were prepared by adding the oil-heptane mixture first to ethanol and then further diluted with DI water. The final volumetric ratio of oil-heptane mixture to ethanol-water mixture was 1 to 40. The time between the sample preparation and measurement was fixed at approximately 10 minutes.[41] The average results were listed in Table 2. SEM images also confirmed that the aggregates are globular. (Supporting Information S1)

Table 2. Characterization of Asphaltene Aggregates Precipitated from Model Oil with *n*-Heptane and Dispersants

Dispersant	Zeta Potential (mV)	Particle Size (μm)
No dispersant	-35 ± 19	1.05 ± 0.22
p-Hexylphenol (*p*C6)	-30 ± 5	0.73 ± 0.12
p-Octylphenol (*p*C8)	-29 ± 8	0.59 ± 0.18
iso-Dodecylphenol (*iso*C12)	-28 ± 6	0.26 ± 0.18
p-Dodecylphenol (*p*C12)	-25 ± 3	0.27 ± 0.17

2.2 Experimental Setup

For microfluidic studies, asphaltene deposition in a porous media microfluidic device was studied by injecting model oil and a precipitant (*n*-heptane) via syringe pumps (Harvard Apparatus PHD 2000) into the device where they are mixed at a T-junction (IDEX, MicroTee Assy PEEK-1/16 in) and then flowed into the porous media, as shown in Figure 1a. The length of 10 cm, between the mixing zone and the porous media, was designed so that no observable asphaltene deposition occurs before the porous media. The time between the

mixing tee and porous media is around two minutes. All experiments were conducted at an ambient temperature of 23°C. The fabrication of the microfluidic porous media, shown in Figure 1b, is described in detail previously.[37] The total flow rate of the fluid mixture was fixed at 60 µl/min (equivalent superficial velocity u = 0.028 m/s). The mass flux of precipitated asphaltenes was approximately 24 g/(s·m^2). The microfluidic device was staged on an inverted microscope (Olympus IX 71), and the visualization of deposition was recorded by a high-speed CMOS camera (Phantom V4.3, Vision Research, Inc.). The images were taken near the entrance of the porous media, assuming the red rectangle shown in Figure 1a. A differential pressure transducer (Validyne P610) was connected to the microfluidic device to measure the pressure drop across the porous media. The experimental images were processed using ImageJ[42] and a Python image-processing module, scikit-image.[43] The procedure was to first identify the location of each post in the porous media by image registration and determine the pixel count associated with asphaltene deposition around each post using Otsu's method.[44] The pixel count was converted to a coverage area.

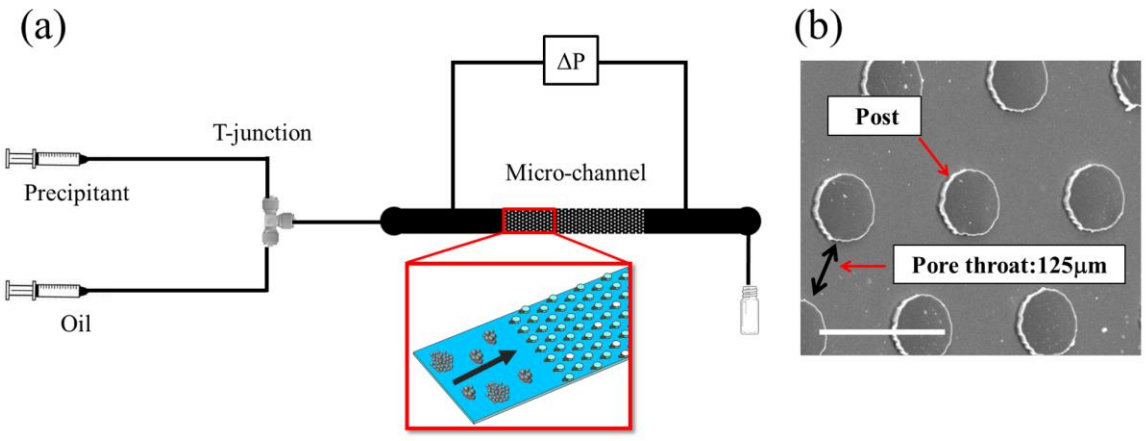

Figure 1. (a) Schematic of experimental setup. (b) SEM image of the porous media used to study deposition. The scale bar is 200 μm. The red rectangle represents the recording region.

2.3 Flow/Aggregate Correlation

Since dispersants alter asphaltene aggregate size, deposition can be described in terms of the Péclet number (Pe), which accounts for the relative contributions from convection and diffusion in the presence of different chemical dispersants, with the limitation that the particles are in the vicinity of an individual post, which acts as the collector surface, and within the size range of 0.1 – 10 μm.[45] The asphaltene aggregate size, obtained from DLS, is used to calculate the Péclet number by Eq. 1-2 to analyze the relative convection-diffusion ratio:[37,45–47]

$$Pe = \frac{2uR_p}{D_{BM}} \tag{1}$$

$$D_{BM} = \frac{k_B T}{6\pi\mu R_p} \tag{2}$$

where R_p is the average radius of asphaltene aggregate, D_{BM} is the Brownian diffusivity (m^2/s) assuming a spherical aggregate which is supported by our SEM measurements, $u = 0.028\ \mathrm{m/s}$ is the superficial velocity, μ is the dynamic viscosity of the oil-precipitant mixture (~0.4 cP), and $k_B = 1.38\times10^{-23}\ (\mathrm{m^2 \cdot kg})/(\mathrm{s^2 \cdot K})$ is the Boltzmann constant.

3. Results and Discussions

3.1 Asphaltene Aggregation with Dispersants

The tendency for asphaltene aggregation is investigated by varying the chain length of the alkyl tail on the dispersant. These chemicals have a phenol head group and an alkyl tail. It is

thought that the alkyl tail increases the steric repulsion between asphaltene aggregates, as shown in Table 2, where smaller aggregates form in the presence of dispersants with longer chain lengths. Goual *et al.* also studied the effects of alkylphenols on asphaltene aggregation and found that aggregates became smaller and filamentary because alkylphenols attached to the surface of asphaltene aggregates, which increased steric interactions.[22] Chang *et al.* conducted a systematic investigation of the effect of dispersants having various functional groups and lengths for the alkyl tail on solubilized asphaltenes. It was found that a longer alkyl tail better stabilized asphaltenes in the solution.[16]

3.2 Deposition Rate and Morphology of Asphaltenes in Micromodel

Asphaltene deposition from model oils with and without the presence of the dispersants was further examined. The representative deposition profiles in porous media are shown in Figure 2. In the absence of the precipitant, shown in Figure 2a, asphaltenes remain soluble in the oil phase and flow within the porous media without depositing. In the presence of the precipitant, *n*-heptane, a cone-shaped deposit is observed to form at the front of the posts, against the flow direction as well as the rear of the posts, as shown in Figure 2b. In the presence of *p*-hexylphenol and *p*-octylphenol, the asphaltene deposits tend to form blunter cone-shape, resulting in a wide streamlined shape, as shown in Figure 2c - 2d versus in the presence of *p*-dodecylphenol and *iso*-dodecylphenol, a smaller streamlined deposit is observed in front of the post. Furthermore, the deposition on the rear-side of the post is significantly reduced in

the presence of dispersants.

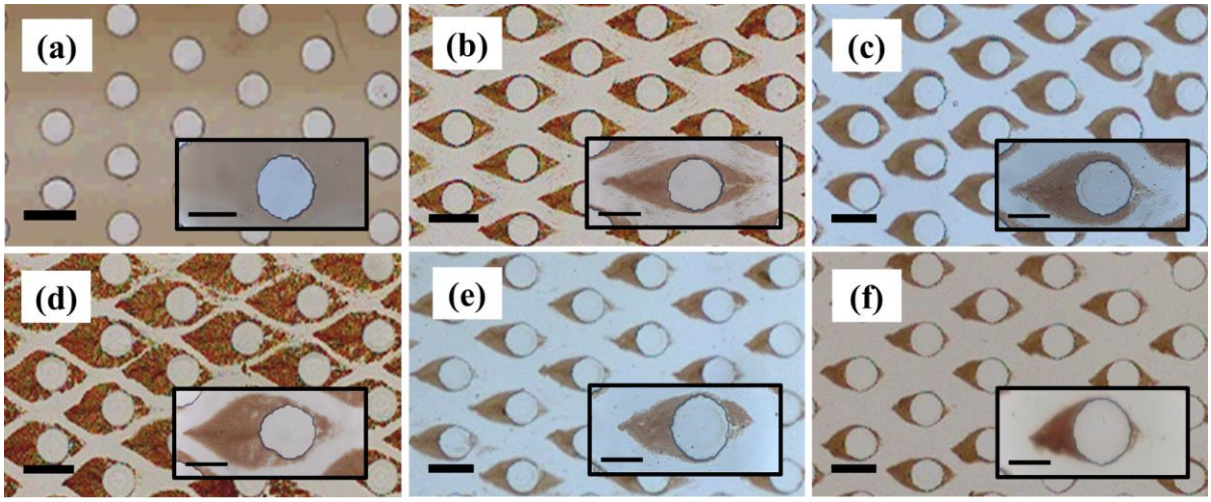

Figure 2. Deposition profiles with and without dispersants in homogeneous porous media taken at 900s near the inlet. (a) Only oil. (b) No dispersant. (c) *p*-hexylphenol (d) *p*-octylphenol (e) *p*-dodecylphenol (f) *iso*-dodecylphenol. Scale bar is 200 μm, and the scale bar in the inset is 100 μm. Flow is from left to right.

The averaged deposition is quantified in Figure 3a, where the deposition rate, the ratio of the coverage of deposited asphaltenes and time, is shown in Figure 3b and the pressure drop measurements are provided in Figure 3c. Model oils with *p*-hexylphenol or *p*-octylphenol show higher overall deposition rates than the no-dispersant experiment. Initially, model oils with *p*-dodecylphenol or *iso*-dodecylphenol also show a higher deposition rate, but the deposition rate then reduces; hence the overall deposition is lower than the no-dispersant case.

The Péclet number (Pe), based on average aggregates size, is calculated to correlate the properties of the flow to the aggregation.[37,46,47] Previous research has shown that stable asphaltenes are present in oil and deposit on the surface as aggregates in the colloidal size range.[4] The no-dispersant case has the highest Pe ($1.7 - 4.2 \times 10^5$). With dispersants, Pe

decreases since the aggregate size decreases. Specifically, Pe ranges from $4.0 \times 10^4 - 1.7 \times 10^5$ for *p*-hexylphenol, 3.0×10^4 - 1.3×10^5 for *p*-octylphenol, $2.1 \times 10^3 - 4.0 \times 10^4$ for *p*-dodecylphenol, and $2.6 \times 10^3 - 4.0 \times 10^4$ for *iso*-dodecylphenol. With a higher Pe, the increased local shear stress exerted on the aggregate is expected to lead to erosion of the asphaltene aggregates[37], leading to the sharper-cone shape observed in Figure 2b. In the experiments with *p*-hexylphenol and *p*-octylphenol, asphaltene deposition increases due to decreased shear stress and increased possibility of attachment due to higher diffusion. However, the deposition rate significantly dropped with both *p*- and *iso*-dodecylphenol, even though the relative ratio of convection to diffusion is the smallest for these dispersants. One possibility is the attractive intermolecular interactions governing asphaltene aggregates have weakened, so that shear stress is better able to erode and shear off these "softened" deposited asphaltenes from the porous media. Further discussion of this possibility will be explored in the following sections. Non-uniform axial deposition profiles are observed along the length of the flow direction, as shown in Figure 4. The reason this occurs is that the asphaltene concentration is being depleted over the distance, which in turn decreases the mass transfer coefficient through the porous media. In Figure 4a, the variation between the first-half and second-half sections is not as obvious as Figure 4b. For larger asphaltene aggregates, the mass transfer entrance region is longer due to lower diffusivity.[48] Therefore, the deposition profile in the presence of *p*-octylphenol has a more prominent difference between these two

sections since the concentration of destabilized asphaltenes decreased faster within the entrance region of the porous media.

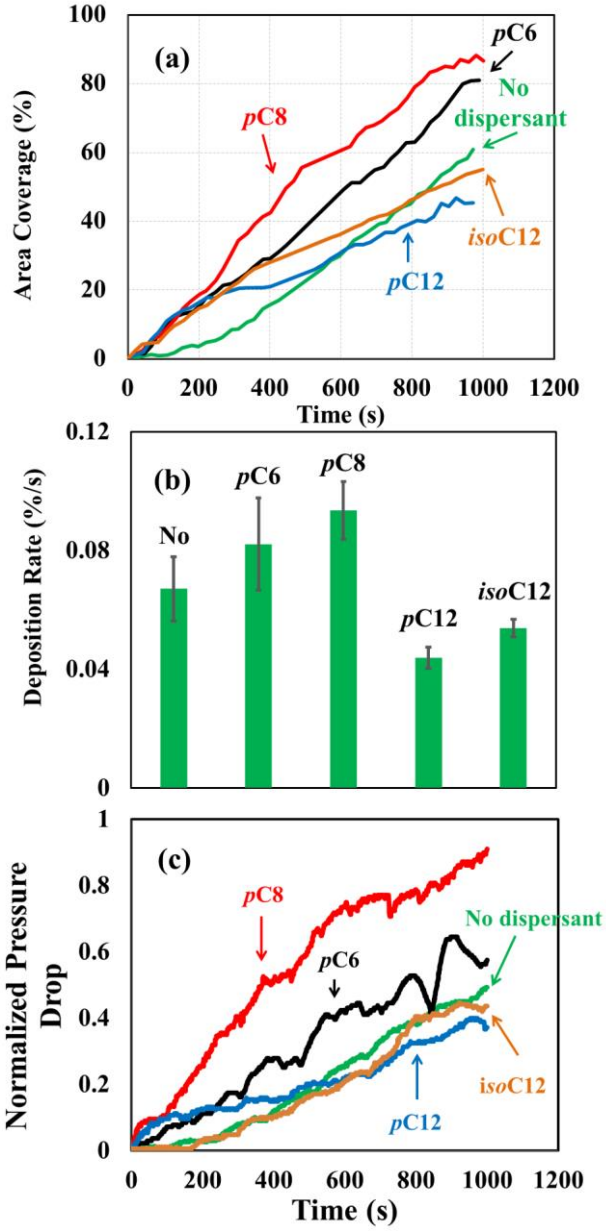

Figure 3. (a) Deposition curves with and without dispersants. The green line represents the oil in the absence of dispersants, black line for *p*-hexylphenol, red line for *p*-octylphenol, blue line for *p*-dodecylphenol, and brown line for *iso*-dodecylphenol. (b) The deposition rate obtained from the linear regression of curves in Figure 3a. (c) The pressure drop measured with flow tests

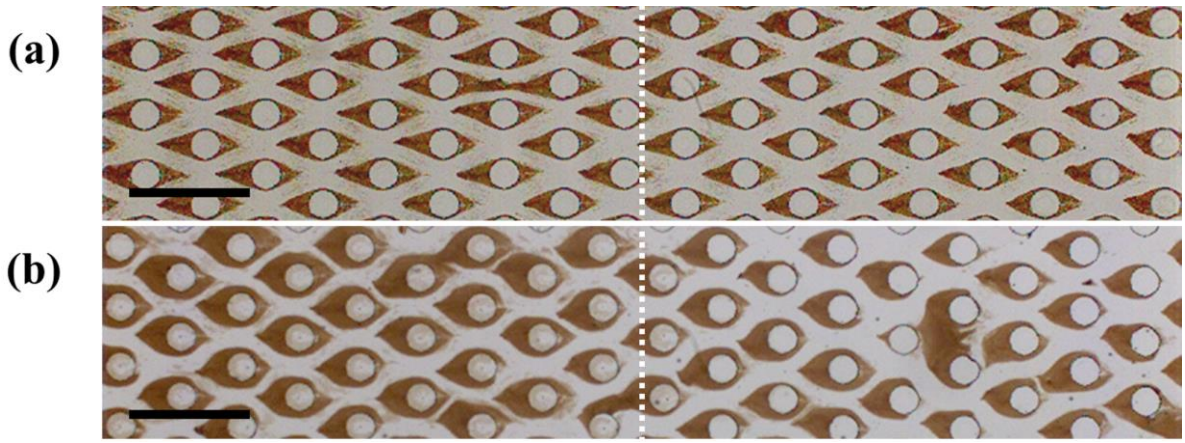

Figure 4. Deposition profiles with and without *p*-octylphenol in taken at 900s. (a) No dispersant. (b) *p*-octylphenol. Scale bar is 500 μm. Flow is from left to right. The white dotted line separates the section near the inlet and the section near the outlet.

3.2 Pore-Scale Visualization of Asphaltene Deposition with Dispersants

The dynamics of the asphaltene deposition at the pore scale are illustrated by deposition growth profiles in Figure 5. Previously, we observed asphaltene deposits form sharper cone-like deposits on the posts when Pe increased.[37] This sharp-cone shape enables a higher shear flow around the deposit, resulting in a competition between attachment and detachment of aggregates. Furthermore, this cone-shape is also present for short times (300s) when octylphenol and dodecylphenol are also added to the model oil. The deposition profile is altered at longer times (600s) in the presence of dispersants in which the deposits experience enhanced detachment. The centerline of the deposits for all three conditions are continuously growing and eroded when confronting the incoming fluid, resulting in a non-linear growth of the asphaltene deposit around a given post. To further investigate the characteristic shape of the deposits (streamlined shape) at the pore scale, local flow patterns (the velocity and shear

rate profiles of the deposits) are plotted by a Lattice-Boltzmann method, as shown in Figure 6 (Described in Supporting Information S2.) High-velocity fluid flow zones are found at the north and south regions of the post ($y =$ 45-90 μm), suggesting a higher shear removal effect. The locations between posts ($x =$ 0-100 μm and 200-250 μm) show the highest velocity. The streamlined shape formed between these two high-velocity zones ($x =$ 100-200 μm) is due to the fluid stagnation region near the post. High shear rates are also found at the interface of the deposit and flowing fluid, resulting in a strong competition between attachment and detachment. However, enhanced local shear stress is not able to explain the decrease in the overall deposition rate for *p*- and *iso*-dodecylphenol. Hence, the intermolecular interactions between asphaltenes in the presence of dispersants are discussed in the following section.

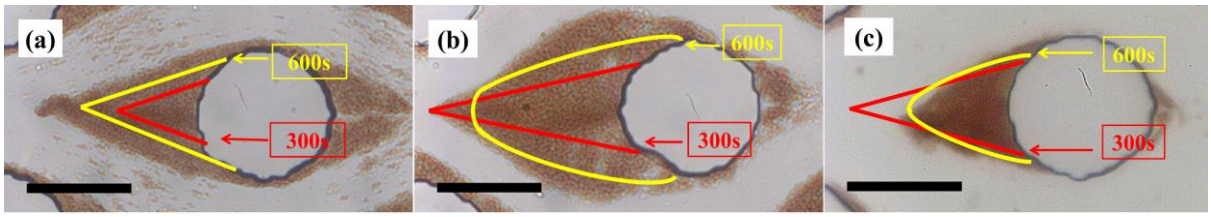

Figure 5. Schematic dynamics of asphaltene deposition growth with and without dispersants. (a) No dispersant (b) *p*-octylphenol (c) *iso*-dodecylphenol. Red line is for 300s. The yellow line is for 600s. Scale bar is 100 μm.

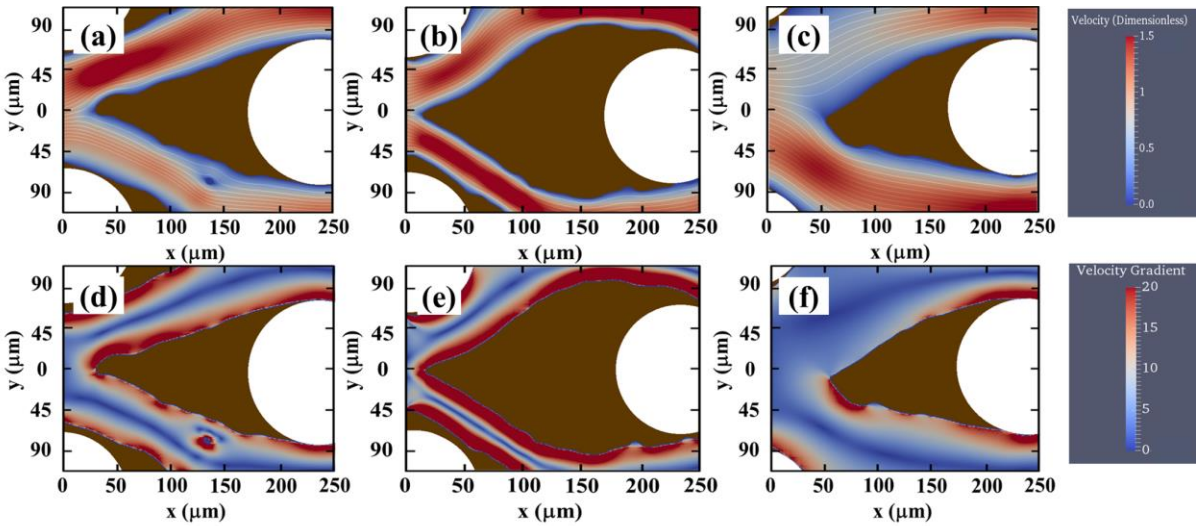

Figure 6. Velocity profile and shear rate around representative asphaltene deposits for no dispersant, *p*-octylphenol, and *iso*-dodecylphenol. Velocity profile: (a) no dispersant, (b) *p*-octylphenol, and (c) *iso*-dodecylphenol. Shear rate: (d) no dispersant, (e) *p*-octylphenol, and (f) *iso*-dodecylphenol. The white area is the post. The brown area is the deposit.

3.3 Forces Between Asphaltene Aggregates

A schematic illustrating the key factors causing asphaltene attachment and erosion is shown in Figure 7. Our hypothesis is that the dispersants increase the steric repulsion between asphaltene aggregates, which influences deposition in two competing ways. The first is by reducing the aggregate size, the asphaltene aggregate diffusivity increases resulting in more collection of aggregates on the posts. The second is by altering the intermolecular interactions between the asphaltene molecules, which can lead to "softer" deposited asphaltenes that are more easily removed by shear forces exerted by flow. The former will cause more deposition while the latter will cause less deposition. Slightly increasing the steric repulsion between asphaltene aggregates cannot sufficiently weaken the aggregate adhesion; hence, octylphenol and dodecylphenol results in more deposition in the porous media.

However, significantly increasing the repulsion between aggregates will more readily enable erosion, leading to less asphaltene deposition. After understanding the deposition tendency for the various dispersants, intermolecular forces are analyzed to better examine the hypothesis.

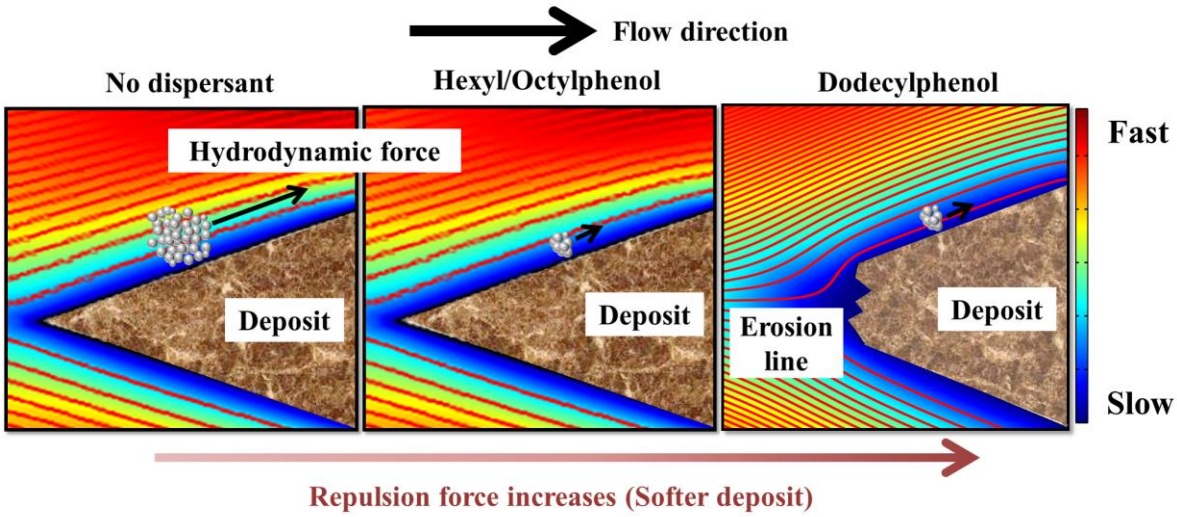

Figure 7. Illustration of detachment of deposited aggregates with 2D velocity distribution with corresponding streamlines.

Asphaltene self-association is governed by the van der Waals attraction with a major contribution from dispersion forces due to induced polarization.[49,50] The dispersion interaction potential (Φ) in an interacting system is the product of the effective Hamaker constant (A) and a function of the geometry of the system. (Eq. 3)

$$\Phi = A \cdot f(geometry) \tag{3}$$

In a system of two macroscopic materials and a given medium, the pair-wise summation is commonly utilized to calculate the effective Hamaker constant.[51–53] Here, the interacting system (subscript ama) consists of asphaltenes in bulk solution (subscript a), medium

(subscript m), and asphaltenes adsorbed onto a surface.[54] If the Hamaker constants for the bulk asphaltenes and adsorbed asphaltenes are assumed to be similar, then the effective Hamaker constant can be calculated as:

$$A_{ama} = \left(\sqrt{A_a} - \sqrt{A_m}\right)^2 \quad (4)$$

where A_a and A_m are Hamaker constants of the bulk asphaltenes and bulk medium solution, respectively. The Hamaker constant of a pure material can be calculated by Eq. 5 with the assumption that the dispersive energy component is the main contribution to the surface energy, which is a good assumption for these experiments due to lack of the hydrogen bonding in solvents (*n*-heptane and toluene):[53]

$$A_m = 24\pi L_0^2 \gamma_s \quad (5)$$

where $L_0 = 0.165\ nm$ is defined as the characteristic distance between interacting molecules, and γ_s is the surface energy. The calculated Hamaker constant ($A_a =$ 5.73 $\times 10^{-20}$ J) was obtained from Gonzalez et al. who used the Lifshitz theory towards a system of asphaltenes.[50] The Hamaker constant of the medium (A_m = 4.22 $\times 10^{-20}$ J) was calculated with the measured surface energy (γ_s = 20.5 ±0.06 mN/m), where the surface tension was measured using a force tensiometer (K100, KRÜSS, GmbH). The effective Hamaker constant of the interacting system (A_{ama}) was estimated to be 1.14 $\times 10^{-21}$ J using Eq. 4. Previously, Fotland *et al.* studied van der Waals forces between asphaltenes by altering the medium with different ratios of *n*-pentane and benzene.[55] They found that the effective

Hamaker constant was reduced with a smaller fraction of *n*-pentane, which also explained their experimental observations that asphaltene precipitation is directly correlated to the ratio of precipitant in the solution. Additionally, Wang *et al.* analyzed the interaction forces of asphaltene surfaces in heptane-toluene mixtures using atomic force microscopy (AFM). They found that the interaction was mainly due to van der Waals attractive forces when asphaltenes were in a solvent with high volume ratio of *n*-heptane, which is similar to the conditions reported here.[56]

To study the attachment and removal of asphaltenes, the attraction and repulsion are estimated as follows. The attraction of asphaltenes to the post is assumed to be a system with a particle and a planar surface in contact with a distance (D), and the attractive force (F_A) can be described by Eq. 6.[53]

$$F_A = \frac{A_{ama} R_p}{6D^2} \tag{6}$$

Since dispersants are known to increase the steric repulsion between asphaltene aggregates by adsorbing onto the asphaltenes, then this steric repulsion has a significant impact on erosion of asphaltene depostited.[16,17,22,24] To evaluate the steric repulsive forces (F_s), we use the force-distance profile between a particle and a repulsive surface, which is shorter than two times of the thickness of the adsorbed layer, ($D < 2L$), estimated by Eq. 7.[53,57,58]

$$F_s(D) = 2\pi R_p \left(\frac{k_B T}{s^3}\right)\left\{\frac{8L}{5}\left[\left(\frac{2L}{D}\right)^{\frac{5}{4}} - 1\right] + \frac{8L}{7}\left[\left(\frac{D}{2L}\right)^{\frac{7}{4}} - 1\right]\right\} \quad for \;\; D < 2L \qquad (7)$$

where s is the average distance between attachment points[59], L is the thickness of the adsorbed dispersant layer. The first term in Eq. 7 is the osmotic repulsion from the overlap of steric surfaces which increases the osmotic pressure and the second term is associated with the loss of entropy associated with adsorption.[57] (See Supporting Information S3) Electrostatic repulsion is neglected because most of the solvents used as the medium are non-polar (*n*-heptane and toluene) and the measured zeta potential for asphaltenes with different dispersants are in a similar range, suggesting that the electrostatic repulsion between asphaltene aggregates are not a dominant factor. The combination of attraction and repulsion forces for different dispersants is plotted in Figure 8.

Retention of aggregates on the surface is presented in two situations. Aggregates can adhere to either *favorable* sites (depositing without repulsive forces) or *unfavorable* sites (with the secondary minimum or overcoming the repulsive barrier staying with the primary minimum). Irreversible deposition occurs at the primary minimum. The combined value of the barrier and the secondary minimum represents the energy for an aggregate to deposit in the primary minimum. Reversible deposition was reported for aggregates depositing with the secondary minimum.[60–63] In Figure 8, the maximum value of the energy barrier increases and the depth of the secondary minimum decreases when the length of the alkyl tail on the dispersant is increased. For aggregates with dodecylphenol, the energy barrier for irreversible

deposition is the highest, and the depth for the reversible process is the shallowest. To further estimate the potential convection effect discussed in previous sections with the interacting forces, the depth of the secondary minimum (reversible deposition) is plotted with the hydrodynamic force as a function of the size of the aggregate. The hydrodynamic force is estimated as the drag force assuming the particle rolling and sliding are the main contributions to the removal as shown in Eq. 8.[64]

$$F_d = 1.7(6\pi)\mu R_p^2\dot{\gamma} \quad (8)$$

The shear rate ($\dot{\gamma} \sim$ 8400 or 1350 $1/s$) is estimated as $(\sim 6u/h)$ where h is the height of the channel or the distance between posts (the pore size).[65] This drag force balances the adhesion force from the secondary well. In Figure 9, the crossover between the drag force based on the height and the secondary minimum shifts with increasing the length of the alkyl tail. This explains the drop in the deposition rate for dodecylphenol. The drag force is also calculated based on the pore size but no crossover is obtained. However, this estimation requires further consideration, including the deformability of the aggregates (changing the contact area) and other removal factors such as lift forces.[66,67] Therefore, more investigations into the rheological properties of asphaltenes and other forces resulted from hydrodynamics are required to analyze the deposition process.

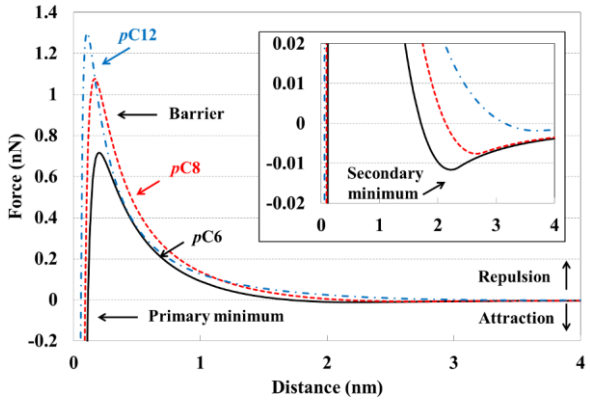

Figure 8. Approximation of the interaction between an asphaltene aggregate and an asphaltene-deposited surface with dispersants. The inset plot is the zoom-in graph of Figure 8. Black line represents *p*-hexylphenol, red dashed line is *p*-octylphenol, and blue dotdashed line is *p*-dodecylphenol.

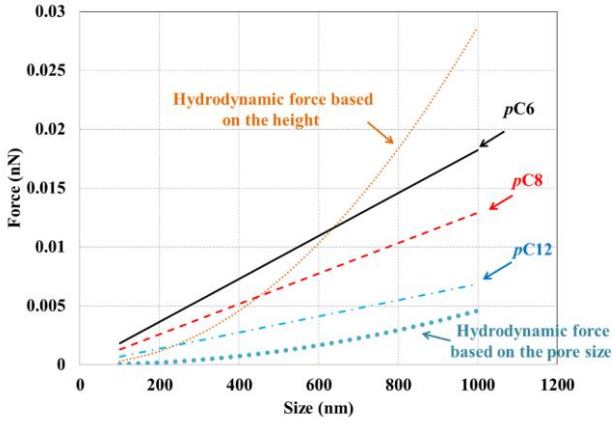

Figure 9. The depth of the secondary minimum and the hydrodynamic force are functions of the size of the asphaltene aggregate. The black line represents *p*-hexylphenol, red dashed line is *p*-octylphenol, and blue dotdashed line is *p*-dodecylphenol. The orange dotted line represents the hydrodynamic force based on the height of the micromodel and aqua dotted line is the hydrodynamic force based on the pore size calculated from Eq. 8.

Microfluidic investigation on the effect of dispersants was also extended to crude oil S, which include asphaltenes along with saturates and resins. The deposition profiles with and without the presence of *p*-octylphenol or *p*-dodecylphenol are shown in Figure 10 at timepoints of 600 and 1200 seconds. The no-dispersant case forms a cone-shape deposition profile, as was observed in the model oil deposition. The profiles in the presence of

dispersants show more streamlined shapes, as shown in Figure 10e and Figure 10f. This streamlined shape is possibly caused by a smaller effective aggregate size. This dynamic growth of deposition is quantified, as shown in Figure 11. More deposition is obtained with the presence of dispersants, which is the same trend observed in the model oil tests. However, the addition of *p*-dodecylphenol caused more deposition than the case with the presence of *p*-octylphenol. There are two possible reasons for this difference. First, there is a significant amount of saturates in crude oil S, which increases the Hamaker constant for the system.[55,56] Hence, the steric repulsion provided by adsorbed dispersants are not strong enough to easily disrupt the deposited asphaltenes due to shear flow. Second, the combination of resins in the crude oil and dispersants stabilize the asphaltenes better in the crude oil compared to the model oil, resulting in even smaller aggregates and less hydrodynamic erosion. Therefore, a higher deposition rate is observed with the presence of *p*-dodecylphenol in crude oil S.

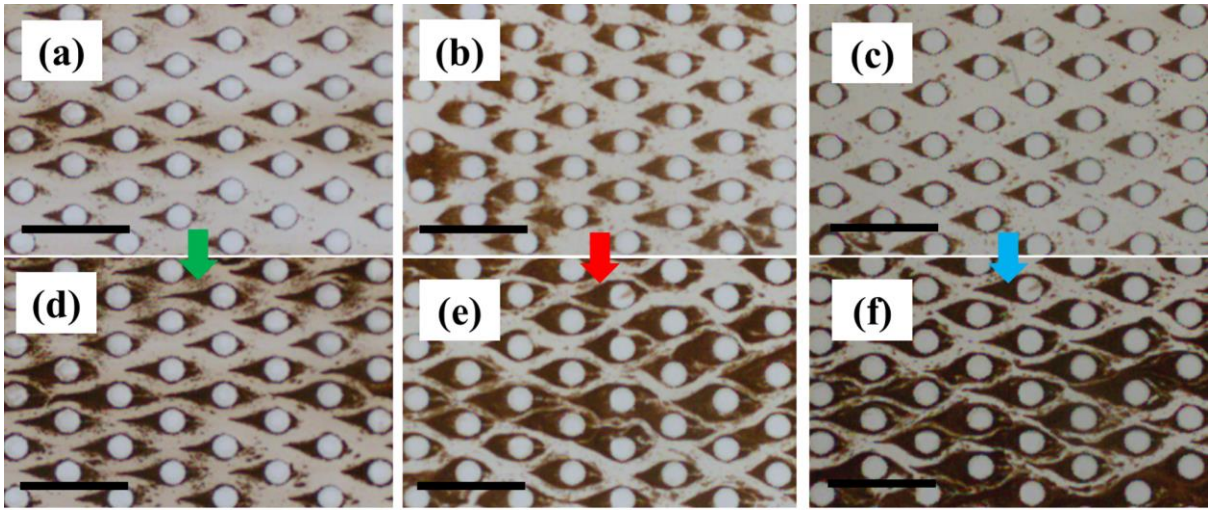

Figure 10. Deposition profiles of crude oil S with and without the presence of dispersants taken at 600s for (a)(b)(c) and 1200s for (d)(e)(f). (a) and (d) are no-dispersant cases. (b) and (e) are for *p*-octylphenol. (c) and (f) are for *p*-dodecylphenol. Scale bar is 500 μm. Flow is from left to right.

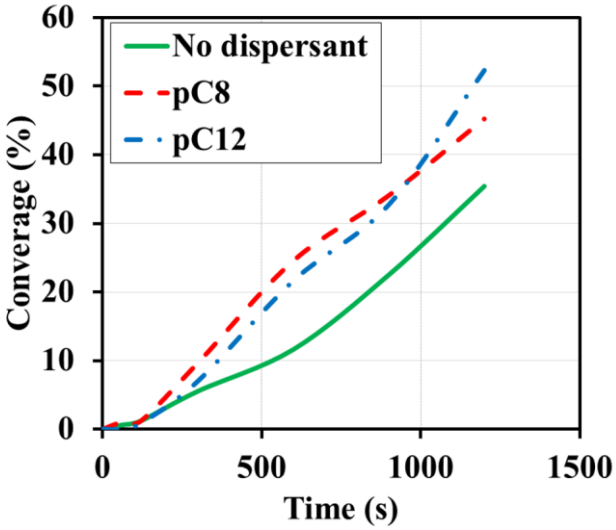

Figure 11. Asphaltene deposition from crude oil in the microfluidic porous media plotted with time with and without the presence of dispersants. The green line represents the crude oil in the absence of dispersants, red dashed line for *p*-octylphenol, and blue dotdashed line for *p*-dodecylphenol.

4. Conclusions

Microfluidic devices offer a well-controlled platform to analyze the relative effects of convection-diffusion and intermolecular forces resulting from chemical injections on the asphaltene deposition. In general, smaller asphaltene aggregates are better able to resist shear flows from the fluid, increasing its probability for deposition. Injection of chemical dispersants effectively reduces their size and resulting in higher initial deposition rates; however, these chemical dispersants alter the intermolecular interactions. Stronger repulsive interactions result in "softer aggregates" that are readily eroded in shear flow after deposition, thereby lowering the overall deposition rate. This is observed for the case with dodecylphenol dispersants and model oil, where the deposited asphaltenes for easily removed by shear forces due to higher repulsive interactions, which eventually resulted in a lower overall deposition

rate. Furthermore, in crude oil systems that include saturates and resins, the asphaltenes are not as easily destabilized compared to the model oil system. The saturates in crude oil increase the attractive Hamaker constant for the asphaltene aggregates, while the resins combined with dispersants reduce the effective aggregate size.

Supporting Information

Images of asphaltene aggregates from optical microscopy and SEM, numerical simulation on flow through porous media, parameters for steric repulsion approximation, and videos of deposition.

Author Information

Corresponding Author

*Email: biswal@rice.edu

Acknowledgments

We acknowledge the financial support provided by the Abu Dhabi National Oil Co. (ADNOC), the Abu Dhabi Oil R&D Sub-Committee, and the Petroleum Institute (PI), UAE. We thank Sun Young Ji, Sang Hun Ji, and Zhuqing Zhang for their technical support.

References

(1) Creek, J. L. *Energy Fuels* **2005**, *19*, 1212.

(2) Mullins, O. C.; Sabbah, H.; Eyssautier, J.; Pomerantz, A. E.; Barré, L.; Andrews, A. B.; Ruiz-Morales, Y.; Mostowfi, F.; McFarlane, R.; Goual, L.; Lepkowicz, R.; Cooper, T.; Orbulescu, J.; Leblanc, R. M.; Edwards, J.; Zare, R. N. *Energy Fuels* **2012**, *26* (7), 3986–4003.

(3) Leontaritis, K. J. Society of Petroleum Engineers, 1989.

(4) Buckley, J. S. *Energy Fuels* **2012**, *26* (7), 4086–4090.
(5) Vargas, F. M.; Garcia-Bermudes, M.; Boggara, M.; Punnapala, S.; Abutaqiya, M.; Mathew, N.; Prasad, S.; Khaleel, A.; Al Rashed, M.; Al Asafen, H. Offshore Technology Conference, 2014.
(6) Zhuang, Y.; Goharzadeh, A.; Lin, Y. J.; Yap, Y. F.; Chai, J. C.; Mathew, N.; Vargas, F.; Biswal, S. L. *J. Pet. Sci. Eng.* **2016**, *145*, 77–82.
(7) Chaisoontornyotin, W.; Haji-Akbari, N.; Fogler, H. S.; Hoepfner, M. P. *Energy Fuels* **2016**, *30* (3), 1979–1986.
(8) Chaisoontornyotin, W.; Bingham, A. W.; Hoepfner, M. P. *Energy Fuels* **2017**.
(9) Novosad, Z.; Costain, T. G. Society of Petroleum Engineers, 1990.
(10) Verdier, S.; Carrier, H.; Andersen, S. I.; Daridon, J.-L. *Energy Fuels* **2006**, *20* (4), 1584–1590.
(11) Pazuki, G. R.; Nikookar, M. *Fuel* **2006**, *85* (7–8), 1083–1086.
(12) Gruesbeck, C.; Collins, R. E. *Soc. Pet. Eng. J.* **1982**, *22* (6), 847–856.
(13) Wang, S.; Civan, F. Society of Petroleum Engineers, 2001.
(14) Tuttle, R. N. *J. Pet. Technol.* **1983**, *35* (6), 1192–1196.
(15) Hu, C.; Yen, A.; Joshi, N.; Hartman, R. L. *Chem. Eng. Sci.* **2016**, *140*, 144–152.
(16) Chang, C.-L.; Fogler, H. S. *Langmuir* **1994**, *10* (6), 1749–1757.
(17) Chang, C.-L.; Fogler, H. S. *Langmuir* **1994**, *10* (6), 1758–1766.
(18) Rocha Junior, L. C.; Ferreira, M. S.; da Silva Ramos, A. C. *J. Pet. Sci. Eng.* **2006**, *51* (1–2), 26–36.
(19) Schantz, S. S.; Stephenson, W. K. Society of Petroleum Engineers, 1991.
(20) Lightford, S. C.; Pitoni, E.; Mauri, L.; Armesi, F. *SPE Prod. Oper.* **2008**, *23* (3), 301–311.
(21) Carlos da Silva Ramos, A.; Haraguchi, L.; Notrispe, F. R.; Loh, W.; Mohamed, R. S. *J. Pet. Sci. Eng.* **2001**, *32* (2–4), 201–216.
(22) Goual, L.; Sedghi, M.; Wang, X.; Zhu, Z. *Langmuir* **2014**, *30* (19), 5394–5403.
(23) Barcenas, M.; Orea, P.; Buenrostro-González, E.; Zamudio-Rivera, L. S.; Duda, Y. *Energy Fuels* **2008**, *22* (3), 1917–1922.
(24) Rogel, E. *Energy Fuels* **2011**, *25* (2), 472–481.
(25) Juyal, P.; Ho, V.; Yen, A.; Allenson, S. J. *Energy Fuels* **2012**, *26* (5), 2631–2640.
(26) Kraiwattanawong, K.; Fogler, H. S.; Gharfeh, S. G.; Singh, P.; Thomason, W. H.; Chavadej, S. *Energy Fuels* **2009**, *23* (3), 1575–1582.
(27) Pereira, J. C.; Delgado-Linares, J.; Briones, A.; Guevara, M.; Scorzza, C.; Salager, J.-L. *Pet. Sci. Technol.* **2011**, *29* (23), 2432–2440.
(28) Melendez-Alvarez, A. A.; Garcia-Bermudes, M.; Tavakkoli, M.; Doherty, R. H.; Meng, S.; Abdallah, D. S.; Vargas, F. M. *Fuel* **2016**, *179*, 210–220.
(29) Hu, C.; Morris, J. E.; Hartman, R. L. *Lab. Chip* **2014**, *14* (12), 2014–2022.

(30) Sieben, V. J.; Tharanivasan, A. K.; Ratulowski, J.; Mostowfi, F. *Lab. Chip* **2015**, *15* (20), 4062–4074.
(31) Doryani, H.; Malayeri, M. R.; Riazi, M. *Fuel* **2016**, *182*, 613–622.
(32) Qi, Z.; Abedini, A.; Lele, P.; Mosavat, N.; Guerrero, A.; Sinton, D. *Fuel* **2017**, *193*, 284–293.
(33) Sieben, V. J.; Tharanivasan, A. K.; Andersen, S. I.; Mostowfi, F. *Energy Fuels* **2016**, *30* (3), 1933–1946.
(34) Kim, M.; Sell, A.; Sinton, D. *Lab. Chip* **2013**, *13* (13), 2508.
(35) Ma, K.; Liontas, R.; Conn, C. A.; Hirasaki, G. J.; Biswal, S. L. *Soft Matter* **2012**, *8* (41), 10669.
(36) Conn, C. A.; Ma, K.; Hirasaki, G. J.; Biswal, S. L. *Lab Chip* **2014**, *14* (20), 3968–3977.
(37) Lin, Y.-J.; He, P.; Tavakkoli, M.; Mathew, N. T.; Fatt, Y. Y.; Chai, J. C.; Goharzadeh, A.; Vargas, F. M.; Biswal, S. L. *Langmuir* **2016**.
(38) Tavakkoli, M.; Grimes, M. R.; Liu, X.; Garcia, C. K.; Correa, S. C.; Cox, Q. J.; Vargas, F. M. *Energy Fuels* **2015**, *29* (5), 2890–2900.
(39) Vilas Bôas Fávero, C.; Maqbool, T.; Hoepfner, M.; Haji-Akbari, N.; Fogler, H. S. *Adv. Colloid Interface Sci.* **2017**, *244*, 267–280.
(40) Mohammadi, S.; Rashidi, F.; Mousavi-Dehghani, S. A.; Ghazanfari, M.-H. *Can. J. Chem. Eng.* **2016**, *94* (9), 1820–1829.
(41) Yudin, I. K.; Anisimov, M. A. In *Asphaltenes, Heavy Oils, and Petroleomics*; Mullins, O. C., Sheu, E. Y., Hammami, A., Marshall, A. G., Eds.; Springer New York: New York, NY, 2007; pp 439–468.
(42) Schneider, C. A.; Rasband, W. S.; Eliceiri, K. W. *Nat. Methods* **2012**, *9* (7), 671–675.
(43) Hunter, J. D. *Comput. Sci. Eng.* **2007**, *9* (3), 90–95.
(44) Nobuyuki, O. *IEEE Trans. Syst. Man Cybern.* **1979**, *9* (1), 62–66.
(45) Adamczyk, Z.; Van De Ven, T. G. . *J. Colloid Interface Sci.* **1981**, *84* (2), 497–518.
(46) Vincent, M. R. de S.; Abkarian, M.; Tabuteau, H. *Soft Matter* **2016**, *12* (4), 1041–1050.
(47) Kusaka, Y.; Duval, J. F. L.; Adachi, Y. *Environ. Sci. Technol.* **2010**, *44* (24), 9413–9418.
(48) Hoepfner, M. P.; Limsakoune, V.; Chuenmeechao, V.; Maqbool, T.; Fogler, H. S. *Energy Fuels* **2013**, *27* (2), 725–735.
(49) Buckley, J. S.; Hirasaki, G. J.; Liu, Y.; Von Drasek, S.; Wang, J.-X.; Gill, B. S. *Pet. Sci. Technol.* **1998**, *16* (3–4), 251–285.
(50) Gonzalez Rodriguez, D. L. Modeling of asphaltene precipitation and deposition tendency using the PC-SAFT equation of state. Ph.D. Thesis, Rice University, 2008.
(51) Vincent, B. *J. Colloid Interface Sci.* **1973**, *42* (2), 270–285.
(52) Kaneda, I.; Vincent, B. *J. Colloid Interface Sci.* **2004**, *274* (1), 49–54.
(53) Israelachvili, J. N. *Intermolecular and surface forces*, 3rd ed.; Academic Press:

Burlington, MA, 2011.
(54) Berg, J. C. *An introduction to interfaces & colloids: the bridge to nanoscience*; World Scientific: Singapore ; Hackensack, NJ, 2010.
(55) Fotland, P.; Askvik, K. M. *Colloids Surf. Physicochem. Eng. Asp.* **2008**, *324* (1–3), 22–27.
(56) Wang, S.; Liu, J.; Zhang, L.; Masliyah, J.; Xu, Z. *Langmuir* **2010**, *26* (1), 183–190.
(57) de Gennes, P. G. *Adv. Colloid Interface Sci.* **1987**, *27* (3–4), 189–209.
(58) Petosa, A. R.; Jaisi, D. P.; Quevedo, I. R.; Elimelech, M.; Tufenkji, N. *Environ. Sci. Technol.* **2010**, *44* (17), 6532–6549.
(59) Rahme, K.; Chen, L.; Hobbs, R. G.; Morris, M. A.; O'Driscoll, C.; Holmes, J. D. *RSC Adv.* **2013**, *3* (17), 6085.
(60) Molnar, I. L.; Johnson, W. P.; Gerhard, J. I.; Willson, C. S.; O'Carroll, D. M. *Water Resour. Res.* **2015**, *51* (9), 6804–6845.
(61) Franchi, A.; O'Melia, C. R. *Environ. Sci. Technol.* **2003**, *37* (6), 1122–1129.
(62) Tufenkji, N.; Elimelech, M. *Langmuir* **2004**, *20* (25), 10818–10828.
(63) Tufenkji, N.; Elimelech, M. *Langmuir* **2005**, *21* (3), 841–852.
(64) Meinders, J. M.; van der Mei, H. C.; Busscher, H. J. *J. Colloid Interface Sci.* **1995**, *176* (2), 329–341.
(65) Hatch, A. C.; Patel, A.; Beer, N. R.; Lee, A. P. *Lab. Chip* **2013**, *13* (7), 1308.
(66) Burdick, G. M.; Berman, N. S.; Beaudoin, S. P. *Thin Solid Films* **2005**, *488* (1–2), 116–123.
(67) Gradoń, L. *Adv. Powder Technol.* **2009**, *20* (1), 17–28.

Graphical Abstract: